Free Energy Analysis of Membrane Pore Formation Process in the Presence of Multiple Melittin Peptides

Yusuke Miyazaki, Susumu Okazaki, Wataru Shinoda*

Department of Materials Chemistry, Nagoya University, Furo-cho, Chikusa-ku, Nagoya, 464-8603, Japan

Abstract

Understanding the molecular mechanism underlying pore formation in lipid membranes by antimicrobial peptides is of great importance in biological sciences as well as in drug design applications. Melittin has been widely studied as a pore forming peptide, though the molecular mechanism for pore formation is still illusive. We examined the free energy barrier for the creation of a pore in lipid membranes with and without multiple melittin peptides. It was found that six melittin peptides significantly stabilized a pore, though a small barrier (a few $k_{\mathrm{B}}T$) for the formation still existed. With five melittin peptides or fewer, the pore formation barrier was much higher, though the established pore was in a local energy minimum. Although seven melittins effectively reduced the free energy barrier, a single melittin peptide left the pore after a long time MD simulation probably because of the overcrowded environment around the bilayer pore. Thus, it is highly selective for the number of melittin peptides to stabilize the membrane pore, as was also suggested by the line tension evaluations. The free energy cost required to insert a single melittin into the membrane is too high to explain the one-by-one insertion mechanism for pore formation, which also supports the collective melittin mechanism for pore formation.

Keywords: pore formation, lipid membrane, free energy, molecular dynamics simulation, melittin, peptide

*Corresponding author

Email address: w.shinoda@chembio.nagoya-u.ac.jp (Wataru Shinoda)

1. Introduction

The fundamental role of biological membranes (lipid membranes) is to work as a partition boundary separating intracellular and extracellular environments, and to maintain physiological activity by regulating substance transport. Membrane defects disrupt such regulation, leading immediately to the crisis of maintaining the biological activity of cells. Such membrane defects can be caused by several possible reasons, such as an external (lateral) tension, a large electric field across the membrane, a shock wave, and importantly antimicrobial peptides (a class of molecules that strongly bind to membrane) [1–3].

Several different mechanisms have been proposed for the antimicrobial action of peptides on membranes, and among them the pore formation mechanism has been extensively studied at a molecular level [4, 5]. In particular, melittin is one of the antimicrobial peptides that have been most extensively studied and is one of the systems in which the molecular theory of pore formation has been mostly investigated [6–24]. Among the wide variety of antimicrobial agents, peptides that insert into the membrane leading to a transmembrane state and forming a toroidal pore are not actually in a major category. Nevertheless, many research works on pore formation by melittin peptides have been conducted using them as model systems that forms pores that can be defined at the molecular level.

However, the details of the energetics or structure of the membrane pores caused by melittin peptides have not been so well understood. The probability of pore formation is greatly dependent on the peptide/lipid (P/L) ratio, namely, a pore hardly opens unless a certain amount of peptides is contained. This suggests that melittin peptides act cooperatively to favor pore formation. Inconsistent experimental measurements of the pore size have been reported: from the dye leakage experiments pore sizes of about 1.25 - 1.5 nm have been described [12], while a larger pore size of about 2.5 nm has been detected by neutron scattering [14]. This discrepancy might be caused by differences in experimental conditions such as P/L ratio or local peptide concentration. Many MD simulations regarding melittin-induced pore formation in lipid membranes have already been performed [25–40]; however, one major problem was pointed out in simulations carried out with the GROMOS force field [26, 30], which has been widely used in the early studies. In these simulations, a too low stability of the helicity of melittin was reported, and the interaction between this peptide and the lipids was possibly over-

estimated. This appears to result in a too easy (with an almost barrierless free energy profile) melittin-induced pore formation when multiple melittin peptides assemble on the lipid bilayer. Recent studies have reported that the CHARMM force field [41, 42] better reproduces experimental physical properties of lipid membranes and melittin helicity on membrane surfaces [43–45]. Thus, we chose this force field to systematically investigate melittin-induced pore formation and pore stability.

The mechanism of pore formation in lipid membranes owing to the presence of peptides such as melittin is generally assumed to be as shown in Fig. 1. First, melittin peptides are adsorbed from the aqueous solution onto the membrane. Then, melittin further stabilizes by folding into a helical conformation on the surface of the membrane because its amphiphilic nature is increased in this conformation. This process has already been reported in previous MD studies [46, 47]. When the density of the melittin adsorbed onto the membrane is large enough to have multiple melittin peptides located at short distances, they assemble to form a toroidal pore. Many previous simulation studies have tried to accidentally capture pore formation using brute-force MD simulations, from which a firm understanding of the molecular process is hardly expected. There is only one systematic study of pore formation and pore stability based on free energy calculations [40]. In this recent study, the free energy profile corresponding to the consecutive insertion of several melittin peptides into a membrane was estimated. Although it was shown that it is necessary to overcome a large free energy barrier for the insertion of the first melittin unit, the subsequent insertion of new units gradually required a lower and lower barrier until the process was found to be almost barrierless starting from the insertion of the 4th or 5th molecule. This result was discussed in terms of a process where melittin peptides act cooperatively to facilitate pore formation.

In this study, a free energy analysis of the cooperative effects of multiple melittin peptides during pore formation in a palmitoyl oleoyl phosphatidylcholine (POPC) lipid membrane by multiple melittin peptides has been undertaken by performing a series of MD simulations with the CHARMM force field. Our simulations elucidated that, when the local melittin concentration is sufficiently high and they are oriented in a radial arrangement, only a very low free energy barrier (a few $k_{\mathrm{B}}T$) must be overcome to form a pore in the membrane. Particularly, it was found that a local assembly of six melittin peptides on the membrane surface drives to a stable pore formation in the membrane. The free energy barrier required to open a pore is sensitive to

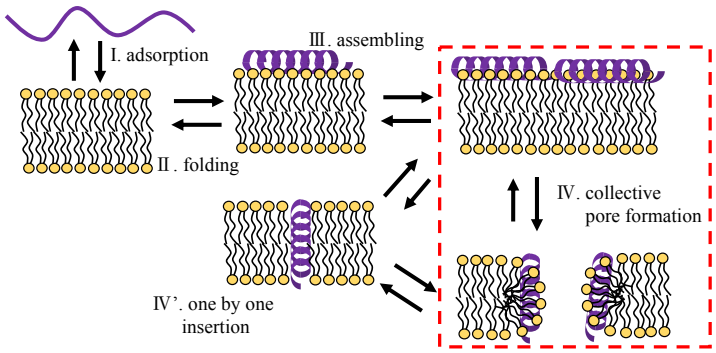

Figure 1: Schematic pore formation mechanism by association of melittin peptides on a lipid bilayer.

changes in the number of melittin peptides surrounding the pore.

The remainder of this paper is organized as follows: In Section 2, we explain the details of the simulations condition including the system setup and free energy calculations to investigate pore formation in lipid membranes. In Section 3, we show results from a series of MD simulations including the free energy calculations and line tension calculations. In Section 4, we discuss the mechanism of pore formation based on the simulation results. Conclusions of this paper are given in Section 5.

2. Methods

2.1. Simulation systems

Five different systems (Systems I-0, I-4, I-5, I-6, and I-7) containing a fully hydrated lipid bilayer composed by 256 POPC molecules in the absence or presence of melittin peptides (in the range 4-7, which corresponds to the suggested number of melittin peptides to form a pore [48]) were built. In these systems, both upper and lower leaflets of the bilayer consisted of 128 POPC molecules. A thick layer of water molecules was necessary to investigate pore formation through free energy calculations. This allowed to minimize the effect caused by interbilayer interactions because, owing to the lateral expansion suffered by the membrane during pore generation, the interbilayer distance was shortened in the course of the free energy calculations. The final number of molecules in the systems is listed in Table 1. We added only counter-ions to neutralize melittin that has a net charge of +6 and no

further addition of salt was considered. This might potentially affect the free energy barrier for a pore formation, because the molecular area of a POPC membrane is reduced and the membrane thickness is increased [49]. However, we assume that physiological salt concentration barely affects a pore formation mechanism. According to experiment investigating effects of ion strength on melittin aggregation in aqueous solution, physiological salt concentration of approximately 150 mM does not influence the aggregation [50]. The initial configuration was prepared using CHARMM-GUI [51]. Each of the melittin peptides, in an α-helical conformation (PDB code:2MLT [52]), was radially disposed on the POPC bilayer with their N-terminus facing each other, as shown in Fig. 2. In the previous studies, it was reported that the N-terminal group of one melittin peptide anchors deeper on the lipid bilayer [36]. It was also suggested that the aforementioned star-like organization of melittin peptides might be advantageous for pore formation [53]. Thus, using this melittin disposition, which appears to be on the ideal arrangement to encourage pore formation, we examine here the effect of multiple melittin peptides on the free energy barrier of this process. Further details on the initial configuration and equilibration MD run for System I are given in Supporting Information.

Table 1: Simulated systems. The number of molecules contained in each simulated system and the simulation times are listed.

simulation	system	melittin	POPC	water	Cl^-	time [μs]
pore formation	I-0	0	256	12800	0	3.78
	I-4	4	256	14652	24	5.04
	I-5	5	256	14946	30	5.04
	I-6	6	256	15042	36	6.72
	I-7	7	256	16329	42	6.72
melittin insertion	II	1	128	4931	6	6.30
brute force MD	III	24	512	25600	144	1.0
line tension	IV-0	0	216	17610	0	1.0
	IV-4	4	216	16619	24	1.0
	IV-6	6	216	16619	36	1.0

Another system (System II) containing a melittin peptide in an α-helical conformation was also built to investigate the free energy required for a

single melittin peptide to penetrate into the POPC membrane. The initial configuration was again prepared using CHARMM-GUI [51].

In addition, a system presenting a much higher P/L ratio (System III) was built. To prepare its initial configuration, 6 melittin peptides were placed on one side of a 128 POPC membrane patch. Then, the system was duplicated along the two axes parallel to the plane of the membrane to generate a larger system (see Table 1). The System III was used to simulate a POPC membrane with highly concentrated melittin coverage.

A final system (System IV), in which the membrane was assembled forming a ribbon-like geometry, was built to measure the line tension of the POPC membrane in the presence/absence of melittin peptides. Further details are given in Section 2.4.

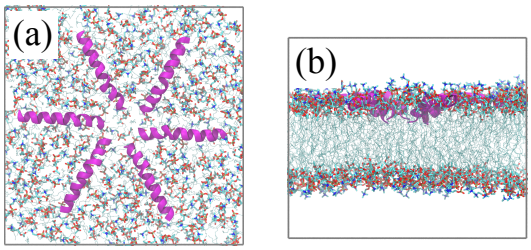

Figure 2: Initial configuration for System I-6. (a) Top view and (b) side view. Water molecules are not shown for clarity. Melittin peptides are shown using a ribbon representation.

2.2. Simulation details

All MD simulations were performed using the GROMACS software package (version 5.0.7) [54]. The CHARMM36 force field [41, 42] was employed for the melittin peptides and POPC. The TIP3P model was used for water [55]. The temperature and pressure were set to 310 K and 1 bar, respectively. A Nosé-Hoover thermostat [56, 57] and a Parrinello-Rahman barostat [58] were used to control the temperature and pressure, respectively. A semi-isotropic coupling scheme, to independently control the pressure in the directions parallel and normal to the bilayer, was employed. Electrostatic interactions were calculated with the particle mesh Ewald (PME) method

[59, 60]. Lenard-Jones interactions were truncated at 1.2 nm with by applying a smooth switching function in the range of 1.0 - 1.2 nm. The LINCS algorithm [61] was used to constraint all bonds involving hydrogen atoms. This allowed us to safely choose a time step size of 2 fs.

2.3. Free energy calculation

To evaluate the energy required to form a pore in the lipid bilayers, the collective variable (ξ) proposed by Tolpekina *et al.* [62], which controls the number density of lipid tail groups in a cylindrical region across the membrane, was employed.

$$\xi = \frac{\Sigma - \Sigma_0}{N - \Sigma_0}, \tag{1}$$

where Σ is defined as

$$\Sigma = \sum_{i=1}^{N} \tanh(r_i/a). \tag{2}$$

Here, N is the total number of lipid tail carbon atoms, $r_i = \sqrt{x_i^2 + y_i^2}$ is the radial distance from the i-th carbon atom to the origin (the center of the pore) in the xy plane of the membrane, and a is a scale parameter that determines the size of the nanopore. We chose $a = 1$ nm. Σ_0 denotes the average of Σ in the equilibrated (non-biased) membrane. Since $\tanh(x)$ approaches to almost 1.0 at $x = 3$, the pore size controlled by ξ reaches $\sim$3 nm at $\xi = 1.0$. This collective variable effectively controls the weighted number density of lipid tail carbon atoms around the pore center but does not control the structure of melittin peptides. In the constraint MD simulations for the free energy calculations, therefore, the melittin configuration emerges naturally as a result of the given control of the collective variable. Umbrella sampling [63] was used to sample over the different values of the collective variable, ξ, in the range from 0.0 to 1.0 and with a spacing of 0.05; namely, 21 umbrella windows were used. The force constant of the bias potential was set to 500 kJ/mol at $\xi = 0$ and was increased by 500 kJ/mol as increasing ξ by 0.05. The weighted histogram analysis method (WHAM) [64] was employed to estimate the free energy profile based on the umbrella sampling data. The simulation time for each window was 120 ns. The data accumulated during the last 90 ns was used for the free energy calculation. The number of lipids included in the systems for the free energy calculation should be carefully chosen to prevent a finite system effect. Hub *et al.* reported that free energy

profiles for pore formation are similar in 128- and 256- lipid systems, though the systems contain no peptides [65]. Thus, 256-lipid systems used in our simulation is large enough to avoid the finite size effects in pore formation process.

For the insertion of a melittin peptide into the POPC membrane (System II), the free energy analysis was also done using WHAM. The distance between the center of mass (COM) of the first three residues of the melittin N-terminus and the center of the lipid membrane along the z-axis was chosen as the collective variable. The initial configurations for each window were created from an equilibrated MD run (in which a melittin was adsorbed on the membrane surface) by pulling the N-terminus at a rate of 0.01 nm/ns. We employed 21 windows for the free energy calculation, and the reference positions of the umbrella potentials were set in the range from -2.0 to 2.0 nm with a spacing of 0.2 nm. For every window, the force constant of the umbrella potential was set to 1000 kJ/mol/nm^2. The equilibration time and sampling time of each window were 600 ns and 150 ns, respectively. The equilibration time was safely selected to be longer than in a previous similar work [33], because an all-atom model rather than a united atom model was used in the present study. The error bars in the free energy profiles represent the standard deviation of several (three or four times) independent free energy samplings.

2.4. Line tension

The System IV was used to measure the effect of melittin on the line tension of the membrane. A membrane having a ribbon-like geometry, under periodic boundary condition, and with a fixed cell length along the ribbon-axis (y-axis) was employed (See Fig.S1) [66]. The membrane normal was disposed along the z-axis; the simulation box was filled with water molecules until they surrounded the ribbon-like membrane, the bilayer edge being exposed to solvent. Because of the line tension of the bilayer edge, the ribbon membranes tend to minimize their line length along the y-axis. We monitored the strength of the pressure along the y-axis at a fixed box length in y-direction, L_y. Pressures along the x and z axes were set to 1 bar by a Parrinello-Rahman barostat (isotropic coupling in x and z directions to prevent random walks of the L_x and L_z). The temperature was set to 310 K using a Nosé-Hoover thermostat. Line tension, Λ, is calculated as;

$$\Lambda = \frac{1}{2}\left\langle L_x L_z \left[\frac{1}{2}(P_{xx} + P_{zz}) - P_{yy}\right]\right\rangle, \tag{3}$$

where L_x and L_z are the cell lengths in x and z directions, respectively, and $\langle \cdots \rangle$ denotes the ensemble average. We carried out the molecular dynamics simulation of the ribbon membrane systems in the $NP_xP_zL_yT$ ensemble. By changing the number of melittin peptides in the system, we evaluated the effect of melittin on the line tension. For melittin-containing systems (System IV-4 and IV-6), the peptides were placed at the bilayer rim with their helical axis perpendicular to the membrane. The MD simulation time was 500 ns for every system, which was long enough to obtain a converged result for the line tension results.

3. Results

3.1. Pore formation free energy

The POPC membrane pore formation free energy profiles in the absence/presence of melittin peptides are plotted as a function of the collective variable, ξ, in Fig. 3. (The histograms calculated from the constraint MD trajectories along the reaction coordinate are also displayed in Fig. S2 to show the quality of sampling.) A clear qualitative difference is found in the free energy profiles of membrane with and without peptides. In pure lipid membranes, without melittin, the free energy continuously increases ξ (Fig.3 (a)).

Table 2: Free energy (FE) differenece between the first local minimum and maximum for each system.

System	FE barrier (kJ/mol)
I-4	47
I-5	18
I-6	7
I-7	6

Figure 4 displays snapshots of the pure membrane system (System I-0) for different ξ values. In the low-ξ region ($\xi < 0.4$), even though the lipid tail density is gradually reduced at larger ξ values, no pore formation is detected. A channel for water penetration through the membranes forms at around $\xi = 0.4$, as shown in Fig. 4(b); at this value, a shoulder appears in the free energy profile. The free energy keeps increasing after the formation of the water

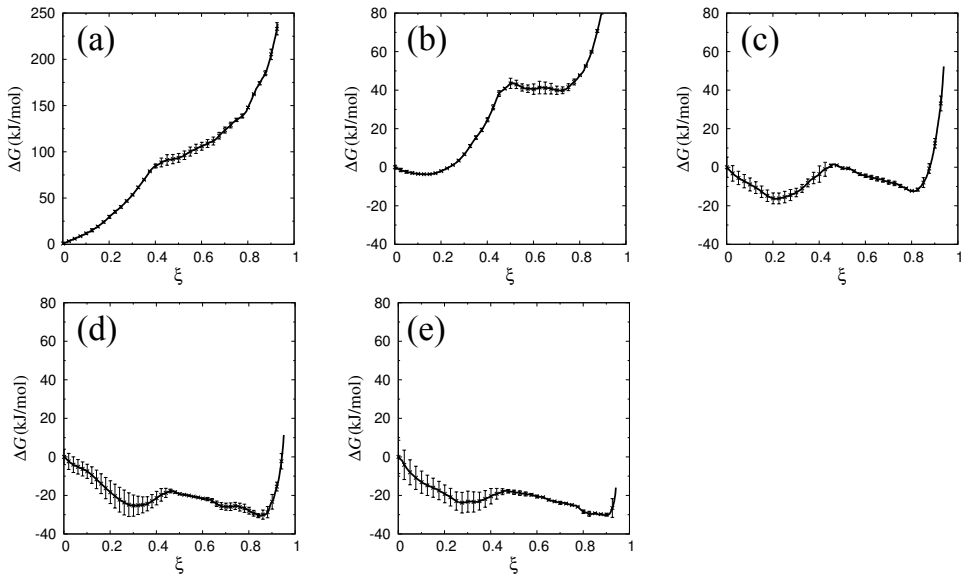

Figure 3: Pore formation free energy in lipid membranes along ξ (a) in the absence of melittin peptide and in the presence of (b) 4, (c) 5, (d) 6, and (e) 7 melittin peptides.

channel at $\xi \sim 0.4$, which indicates that the pore cannot be stabilized in the absence of peptides. It is clear from Fig. 4 that the membrane pore formed along the collective variable is always hydrophilic; the lipid headgroups are oriented towards the pore surface. In the high-ξ region ($\xi > 0.5$), after pore formation, the radius of the toroidal pore expands laterally as ξ increases. The free energy minimum is only found at $\xi = 0$, clearly demonstrating that the unperturbed membrane is the only stable state for the pure membrane.

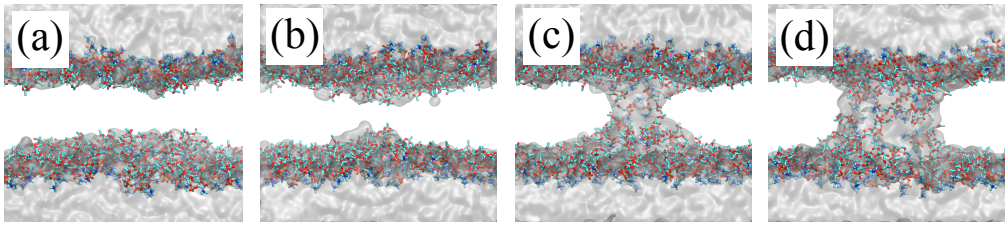

Figure 4: Snapshots extracted from the MD simulations of System I-0 at different values of the collective variable: (a) $\xi = 0.2$, (b) $\xi = 0.4$, (c) $\xi = 0.6$, and (d) $\xi = 0.8$. Water region is drawn as a grey transparent contour, and lipid headgroups are represented as thick lines.

On the contrary, the free energy profiles estimated in the presence of multiple melittin peptides show two free energy minima. The first one, at a small (but not zero) ξ value ($\xi < 0.4$), indicates that the lipid density is spontaneously reduced by the existence of melittin peptides on the membrane surface. For the System I-6, this can be seen in the snapshot in Fig. 5(a), where the melittin peptides that deeply penetrated push the lipids laterally to some extent. The ξ value at which the first minimum on the free energy profiles is located increases with the number of melittin peptides. This suggests that the membrane is laterally stretched as a result of the adsorption of multiple peptides on its surface. Table 3 lists the averaged molecular area at the first free energy minimum for each membrane system. The results clearly show that the adsorbed melittin peptides effectively expand laterally the lipid membrane; in other words, the membrane is effectively thinned by melittin adsorption. This should contribute to reduce the free energy barrier for pore formation (see Fig.2). The second energy minimum is found at larger ξ values ($\xi >0.5$) shows that the membrane pore is significantly stabilized by multiple melittin peptides. Figure 5(b) shows a snapshot taken at around the transition state region, when a water channel formation is about to take

place. At $\xi = 0.6$ (Fig. 5(c)), the melittin peptides have bridged through the membrane. As is clear from Fig. 3, once a pore forms, the free energy gradient drives the pore growth to the energy minimum at $\xi = 0.89$ (shown in Fig. 5(d)). The ξ values at the second free energy minimum reflect the stable pore sizes, which depends on the number of assembled peptides. The depth of the second free energy minimum is largely changed depending on the number of peptides. For the System I-4, the free energy barrier that has to be overcome to reach the pore formation is significantly high (>50 kJ/mol), and the free energy gain after the pore formation is small (Fig. 3(b)). This suggests that we can find a pore in the presence of four melittin peptides, though the driving force required to attain the formation of the pore is significant and the resultant pore stability is low. The situation is largely changed by increasing the number of melittin peptides. With five melittin peptides, the pore stability is significantly improved. The free energy value at the second minimum (pore state) is almost identical to that found for the first minimum (pre-pore state) at $\xi = 0.2$. The free energy barrier (about 15 kJ/mol) is also significantly reduced. The stability of the pore is higher in the presence of six or seven melittin peptides (Systems I-6 and I-7). In these systems, the pore state is more stable than the pre-pore state, though a free energy barrier of a few $k_{\mathrm{B}}T$ is still observed. To confirm the accuracy of the obtained free energy profile, a series of MD simulations were started from configurations in the transition state region using random velocities taken from a Maxwell distribution at 310 K. Twenty different initial structures corresponding to $\xi = 0.47$ were employed, and half of the MD simulations ended up in the pore state while the other half finished in the pre-pore state within 200 ns. These additional MD simulations clearly demonstrates that a small but meaningful free energy barrier still exists between the pre-pore and pore states in the presence of 6 melittin peptides and the isocommitter surface is found around $\xi = 0.47$.

In the transition state region, the membrane structure at the place in which the water channel is formed in the presence of melittin peptides (Fig. 5(b)) is different from that in the absence of melittin (Fig. 4(b)). This is clearly observed in the probability density maps of the lipid hydrophobic core (Fig. 6). In melittin-free membrane, a symmetric membrane is thinned out in the controlling volume. In the presence of melittin, however, the melittin-adsorbed leaflet solely deforms as a result of its strong interaction with the melittin peptides. The lipid molecules around the locally deformed lipid leaflet extend their hydrophobic tails toward the other leaflet. The opposite

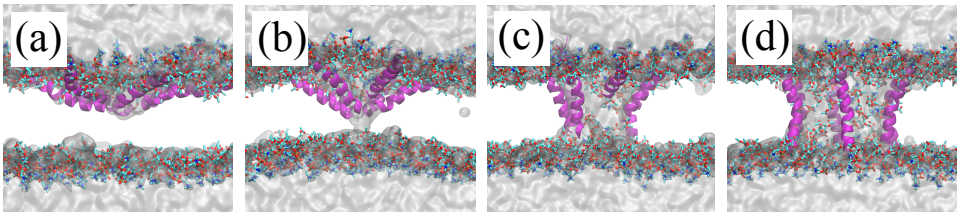

Figure 5: Snapshots extracted from the MD simulation of System I-6 (POPC lipid bilayer in the presence of six melittin peptides) at different values of the collective variable: (a) ξ =0.30, (b) ξ =0.43, (c) ξ =0.60, and (d) ξ =0.89. Water and lipid headgroups are drawn in the same way as in Fig. 4. Melittin peptides are represented by magenta ribbon.

Table 3: Averaged molecular area per lipid at the pre-pore stable state for each system.

System	Area (nm^2)
I-0	0.656±0.009
I-4	0.694±0.009
I-5	0.710±0.015
I-6	0.723±0.010
I-7	0.743±0.014

leaflet is stretched only laterally, partly because of the interdigitation of the hydrophobic tails. At this stage, the deformed membrane is frustrated by the local stress, which leads to a free energy barrier for the pore formation even in the presence of multiple melittin peptides. When a water channel penetrates through the membrane, the deeply inserted melittin N-termini, composed by positively charged glycine residues, come into contact with the phosphate groups of the lipids in the opposite leaflet (see Fig. 7). The Coulomb energy gain because of this association stabilizes the water channel, producing a driving force that expands the pore laterally. Once this process takes place, there is no free energy barrier to form a stable pore of a certain pore size.

Additionally, we examined our assumption that physiological salt concentration barely affects a pore formation free energy. The calculated free energy profiles for System I-6 were comparable to each other with (150 mM NaCl) and without salt (Fig. S3). The results are consistent with a previous observation [50]. Moreover, we checked the finite size effect in free energy calculation for a pore formation process in the presence of multiple melittin peptides (Fig. S4). A free energy barrier to induce a pore in the presence of six melittin peptides is within errors of the free energy profile for System I-6, which indicates systems consisting of 256-lipids are large enough to avoid an artifact due to the periodic boundary condition in the free energy calculation.

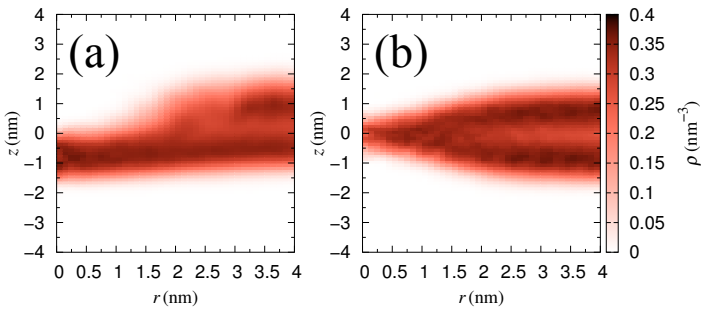

Figure 6: Density maps of lipid tails in cylindrical coordinate in the presence and absence of six melittin peptides. (a) System I-6 at ξ =0.43 and (b) System I-0 at ξ =0.43.

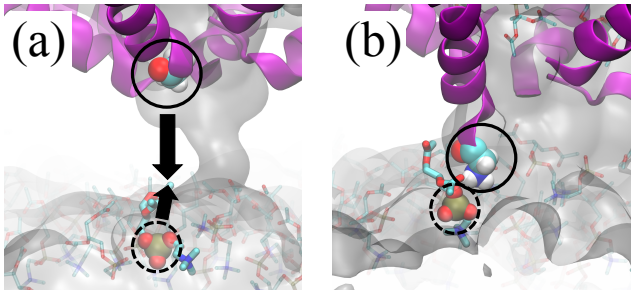

Figure 7: Snapshots from the MD simulation for System I-6 started near the transition state. The N-terminal glycine surrounded by a black circle associated with the phosphate of POPC lipid in the other leaflet surrounded by a dotted circle. The color code is the same as Fig. 4. (a) A closer look of Fig. 5(b) at the transition state, and (b) just after the association of the glycine residue with the phosphate group as a result of deep insertion of the melittin peptide into the bilayer.

3.2. Pore structure

As shown in Fig. 3, stable pore states were found at characteristic values of the collective variable, ξ, in Systems I-4, I-5, I-6, and I-7. In order to investigate their structure, additional 1 μs-long non-biased MD simulations were started from the pore states. As suggested from the free energy profiles, the pore structures were maintained, and all melittin peptides stayed around the membrane rim except in the case of System I-7, in which one of the seven melittin peptides has eventually escaped from the pore region after 0.5 μs. Thus, the structural analysis of the pores was carried out using 1μs MD trajectories for the Systems I-4, I-5, and I-6, but only the first 0.5 μs MD trajectory for System I-7. In all systems, the stable pores were found to be of toroidal type, though thermal fluctuations were not small. Figure 8 displays the probability density plots of the lipid headgroups (PH, phosphate segments) in the cylindrical coordinate for System I-6. It clearly shows that the lipids around the pore reorient their headgroups toward the aqueous phase to make the pore hydrophilic. All peptide helices orient perpendicularly to the membrane surface when they are associated to the pore, as shown in Fig. 5(d).

In free energy profiles, the stable pore states are found at different ξ

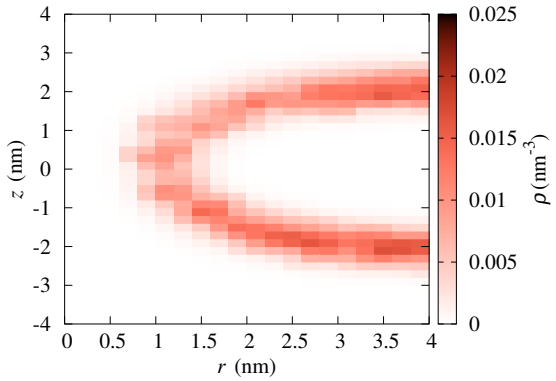

Figure 8: Number density of lipid headgroups (phosphate segments) around the stable pore.

values depending on the number of melittin peptides around the pore. This suggests that the stable pore size varies with the number of melittin peptides. To estimate the pore sizes, we calculated the number density of the lipid tail particles along the radial direction in the cylindrical coordinate using the pore center as origin. The results are given in Fig. 9. To quantify the pore radius, we measured the radial distance at which the number density first reaches the half of the maximum. The estimated pore radii are 1.57±0.04, 1.92±0.03, 2.22±0.05, and 2.34±0.05 nm for the Systems I-4, I-5, I-6, and I-7, respectively. As the number of melittin peptides increases, the pore radius increases. However, the increase in the radius of the pore when passing from 6 to 7 melittins is smaller than those found when passing from 4 to 5 or from 5 to 6 melittins. Especially, the obtained radius in the presence of the 6 melittins (System I-6) shows a good agreement with the experimental value of 2.2 nm for stabilized melittin pores in dehydrated DSPC membranes [48].

In contrast to our results, a recent MD study showed that a pore by six melittin peptides was not so stable in dimyristoyl phosphatidylcholine (DMPC) bilayers[67]. The discrepancy may come from the initial configuration, because the pore size showed a rapid change at the initial stage of the MD simulation[67]. In our MD simulation with a stable pore in System I-6, the pore structure was obtained from the free energy calculation of pore formation, started from surface adsorbed melittin peptides structure. There-

fore, the starting configuration is probably well equilibrated, compared to that used in the previous study[67].

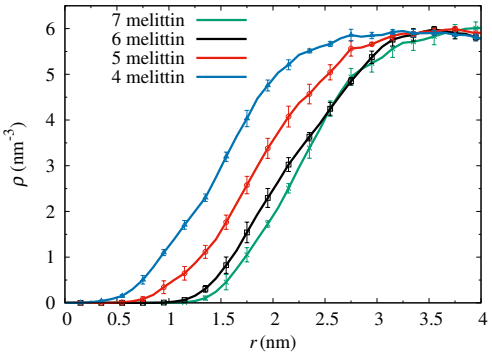

Figure 9: Number density of lipid tail particles along lateral radial distance.

3.3. Line tension

We evaluated how melittin peptides effectively reduce the line tension of POPC bilayer using Systems IV. All melittin peptides were entrapped at the bilayer edge, which should contribute to reduce the line tension to some extent. Table 4 lists the line tension values as a function of the number of melittin peptides introduced in the system. In the pure POPC membrane, the line tension was estimated to be 35 pN, which is in good agreement with the experimental values ($8 - 42$ pN) [68]. A previous CG-MD simulation predicts a line tension of 25 pN for a DMPC membrane [69]. This could be explained by the difference in the thickness of the membranes; namely, the thicker POPC membrane shows a higher line tension than the thinner DMPC membrane. Line tension values decreased significantly when melittin is present at the bilayer rim. However, even if the number of melittin peptides is large enough to fully cover the bilayer edge, the line tension is not zero, but shows a value of about 20 pN. When we place 6 melittin peptides along the bilayer rim (System IV-6), the local concentration of melittin peptides at the bilayer rim is higher than that needed to form the stable pore in System I-6. Thus, melittin peptides seem not fully stabilize the "straight" bilayer edge, as in the ribbon system, in terms of line tension. This reflects the

fact that melittin has much smaller hydrophilic face of the helix compared to hydrophobic one; which suggests the melittin has preferred curvature of bilayer edge to stabilize. This is an obvious indication that melittin is a pore-forming peptide in lipid membranes.

Table 4: Calculated line tension of the ribbon-like POPC bilayer for each system.

System	Line tension (pN)
IV-0	35.1
IV-4	23.2
IV-6	20.5

3.4. Free energy barrier for the insertion of an adsorbed melittin peptide into the lipid membrane

In the previous sections, we described the cooperative insertion of multiple melittin peptides into the membrane to form a pore. An alternative process that could in principle take place is a one-by-one insertion. This motivated us to investigate the free energy barrier for this process.

First, we ran a long-time (1 μs) unbiased MD simulation of a single melittin peptide on a POPC membrane. Although a few different melittin orientations were tried as initial configurations, all of them ended up with melittin adsorbed on the POPC membrane and always adopting a similar configuration. No spontaneous melittin penetration through the membrane was observed during the simulation. Figure 10 shows the distance between each residue of the adsorbed melittin peptide and the bilayer center along the bilayer normal z. The melittin C-terminus (res. no. 21 – 26) resides near the membrane surface, at which the distance between the membrane center and the lipid headgroups is $\sim$ 1.9 nm, because of the interaction formed between the three charged Lys residues present in this region with the lipid headgroups, while its N-terminal part (residues 1–14) penetrates deeply into the membrane, disturbing the hydrophobic core of the lipid bilayer (note that the z-coordinate of the esters linked to the glycerol groups is around 1 nm). However, these residues do not translocate to the opposite leaflet; no bridging state was spontaneously attained during the MD simulation.

To quantify the energy that a melittin peptide needs to penetrate through the membrane, we calculated the free energy as a function of the z-projected

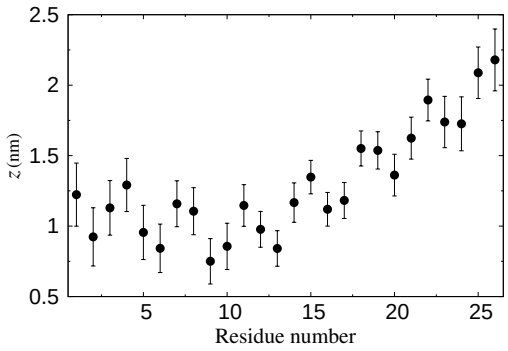

Figure 10: Membrane normal distance between each residue of melittin and the center of a POPC membrane. The first residue is the N-terminal of melittin (glycine). The last terminal is the C-terminal of melittin (glutamine). The ninth residue, leucine, is the most deeply embedded during the simulation.

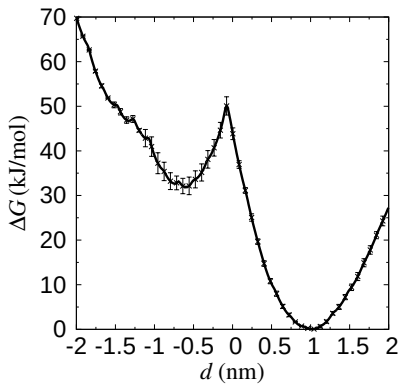

Figure 11: Free energy profile for the insertion of one melittin peptide. The horizontal axis shows the distance between the center of mass of the first three residues of the N-terminal part of one melittin and the center of the POPC membrane core. The local minima at $d = -0.6$ and 1.0 nm show that the melittin peptide is in a transmembrane state and membrane surface state, respectively.

distance between the COM of the first three residues of the N-terminal group and the bilayer center (d). As seen from Fig. 10, in a stable adsorbed state of the melittin, the COM of the first three residues is found at $d \sim 1$ nm. This is confirmed in the free energy profile shown in Fig. 11 (System II). Figure S5 shows the snapshots of System II during the free energy calculation at the transmembrane, transition, and surface adsorbed states. We observe a rapid increase in the free energy as the controlled melittin segments move deeper ($d \sim 0$ nm) into the membrane. Another free energy minimum is found at $d \sim -0.6$ nm. This one corresponds to the bridging state of melittin across the membrane, where the charged N-terminal segments penetrated through the membrane and contacted to the lipid headgroups in the other leaflet. A large free energy barrier of 50 kJ/mol is observed at $d \sim 0$ nm. As shown in Fig. S5(b), at this state, the penetration of the charged N-terminal region into the bilayer center causes water penetration into the bilayer. This explains the large energy barrier found for this process. The free energy barrier is similar to that observed in an earlier work, where a different united atom force field (GROMOS) was adopted instead [33]. The bridged state of melittin is supposed to be attained first in the one-by-one insertion process. However, the estimated free energy barrier suggests that the event quite rarely happens.

4. Discussion

4.1. Mechanism of pore formation

The free energy analysis presented in this paper basically compares the free energy barrier required to create a pore in a membrane in the presence of multiple melittin peptides with that needed in their absence. In the presence of multiple melittin peptides (4 to 7), two free energy minima are detected along the collective variable, ξ. They correspond to a pre-pore state, where adsorbed melittins are assembled on the membrane, and a pore state. The free energy barrier that must be overcome to form a pore is high in case of four melittins; however, this barrier is significantly smaller (of the order of a few $k_{\mathrm{B}}T$) in the presence of more than five melittin peptides. From the free energy profiles, it can also be suggested that once the pore state is attained, the pores show high stability. In the free energy calculations, we assumed that the multiple melittin peptides disposed initially on the membrane surface are radially aligned and with their N-termini facing each other; this structure is supposed to be beneficial for a pore formation. Since we did

not include melittin positions as collective variables, the obtained free energy profile is supposed to depend on the initial configuration of melittin. We examined how high/low the free energy barrier for a pore formation in a POPC membrane with an ideal melittin configuration is. Ideally, we had to compute the free energy required to have the aforementioned melittin disposition on the membrane. In fact, we have also conducted free energy calculations for System I-6 with different orientations of melittin peptides on the membrane surface; (1) all melittin C-termini facing each other, and (2) six melittins alternatively orient C- or N-termini toward the pore center. In case of (1), some melittin peptides were easily escaped from the pore region during the free energy simulation, thus, those melittins cannot contribute to the pore formation free energy (Fig. S6(a)). Since melittin has net charges of +1 and +4 in its N- and C-termini, respectively, the strong repulsive electrostatic interaction among C-termini destabilized this peptide arrangement. Furthermore, the C-terminus is not deeply inserted into the bilayer as shown in Fig. 10, which suggests that the peptide alignment in (1) is not preferred to contribute to a pore formation. Thus, since the melittin peptide pointing the C-terminal toward the pore center does not show attraction to the pore, the motions of melittin peptides to the biased membrane are out of control with the present collective variable defined by lipid tails. This gives rise to a significant statistical error in the free energy estimation. We have also attempted the free energy simulation with a wall potential to prevent the melittin escape, though this guiding potential costed additional free energy, which was also difficult to be estimated accurately due to a significant statistical noise. Even in case of (2), a similar problem was observed; the peptides pointing the C-terminus to the pore center was often escaped from the pore region (Fig. S6(b)). Therefore, the pore formation free energy by the specified number of melittin can be successfully estimated in the case of melittin N-termini facing each other in an initial configuration so as to contribute all the melittin to the pore formation. Although the star-like configuration is entropically unfavorable, the probability of occurrence of the configuration could be larger as increasing concentration of the melittin peptides. The configuration in that melittin N-termini facing each other has the smallest electrostatic repulsion among the star-like configurations. The electrostatic energy cost that is required to orient one melittin C-terminus toward the pore center in the configuration is roughly estimated to be $\sim$50 kJ/mol with a simple peptide model. In addition, the adsorption of melittin causes a deformation of the lipid bilayer with deeply inserted N-terminus.

From the viewpoint of membrane deformation energy, assembly of N-termini should be more beneficial. This also encourages the star-like assembly of melittin peptides with N-termini around the pore center. Free energy estimation for peptide assemblying process is not straightforward because we should consider the complex effects of membrane deformation by melittin and screening effect by water and lipid headgroups. Although this task could be investigated in the future using coarse-grained MD simulations [70–72], it is prohibitively expensive for all-atom MD simulations.

Despite this issue, a clear result is that the free energy barrier for pore formation via the cooperative insertion of six or seven melittins into the membrane is significantly smaller than that required for a melittin to penetrate through the membrane and form a bridging state. It is also clear that a single melittin at the surface points the N terminus into the membrane core deeply, lowering the local density of lipids in the membrane. In addition, melittin clustering causes a greater influence on the local lipid density, which changes the location of stable state to a larger value of the collective variable, ξ. Water channel formation is a key event that takes place in the transition state region and leads to pore formation; pore formation is induced along the free energy gradient once the water channel is established. A small free energy barrier was still detected even in the presence of six or seven melittin peptides initially placed following the previously described radial alignment on the membrane. This explains the difficulty of directly observing pore formation during the simulation time.

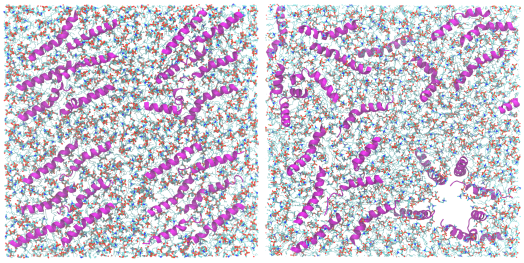

Figure 12: Top view of System III at the initial and final (0.6 μs later) configurations.

We have carried out a large-scale trial MD simulation of a bilayer com-

posed by 512 POPC lipids with a concentration of melittin high enough to expect pore formation. In the initial configuration, six melittin peptides were placed randomly on a POPC bilayer form by 128 lipids, which was then duplicated along both x and y directions to lead to four similar peptide arrangements. Nevertheless, only a pore out of the four was generated in a relatively early time ($\sim$30 ns), as shown in Fig. 12. The presence of multiple melittins in sufficiently high concentration is not the only condition leading to pore formation. This could be partly because a free energy barrier was still detected even with an ideally arrangement of melittin peptides (*e.g.*, System I-6). After 200 ns of the trial MD simulation, the pore was completely formed with six melittin peptides that were adsorbed on the edge of the pore and perpendicular to the lipid bilayer, and then stable for 600 ns. It is notable that the observed pore formation process was a collective one. In fact, when the pore formation was initiated, the N-termini of the six melittin peptides around the formed pore center were cooperatively inserted into the lipid bilayer as we obserbed in the free energy calculation (Fig. 5). No melittin peptides were inserted alone into the bilayer before the pore formation.

The free energy calculations demonstrated that the pore formation process most likely takes place because of the presence of multiple melittin peptides as a collective phenomenon. Thus, it was suggested that the one-by-one melittin insertion process might not be an effective way to initiate pore formation. However, once a pore is opened by multiple melittins, the free energy barrier for another melittin to join the bridge (pore) state should be much lower than that for initial (before pore formation) melittin insertion [40]. Thus, after attaining pore formation, the free energy barriers for the exchange between melittin members to support the pore might be lower. However, according to the free energy profile in Fig. 3, if the number of melittin peptides in the pore edge is reduced to five or four, the pre-pore state is preferred to the pore state, The present MD results demonstrate that pore formation is considerably advantageous if six melittin peptides are present. Even though the free energy profile computed in the presence of seven melittins was similar to that in the presence of six melittins, a long MD simulation suggested that the seven-membered pore is already a little overcrowded, and one melittin left the pore during the simulation. A pore formation free energy calculation in the presence of 8 melittin peptides was also attempted in this work. In this case, it was very difficult for the eight molecules to remain aligned radially, and one or two melittin peptides diffused away immediately during the simulations. This is mainly due to the existence of significant repulsive

electrostatic interactions among the charged residues of melittin peptides at this overcrowded situation. On the other hand, in the case of 4 melittins, the opened pore is too narrow to stabilize a water channel, and the stability of the pore state is reduced. A trial free energy simulation including 3 melittin peptides (not shown in the result section) shows that the stability of pore state is further reduced and the free energy minimum at $\xi > 0.4$ is vanished. From these observations, stable pore formation is found to be encouraged by the aggregation of about 6 melittin peptides on the membrane surface. In addition, the radius of the pore made by about 6 melittin molecules is plausibly the most suitable one so that the melittin molecules at the bridge state can support the bilayer edge. Line tension calculations also evidence the importance of effectively stabilizing pore curvature by the adsorption of melittin onto the bilayer rim.

Finally, it is worth mentioning that, according to experimental study on the mechanism of membrane permeabilizing peptides [24], pores formed by melittin are supposed to be transient. Pores formed by 5−7 melittin peptides, however, are apparently stable in the obtained free energy profiles (Fig. 3). This is just because we explore the free energy landscape with a restriction of the number of melittin peptides contributing to the pore formation. As shown in Fig. 1, there might be an alternative pathway to make a pore by one-by-one melittin insertion. Free energy difference for variation of the number of the melittin peptides forming a pore has been studied by Lyu *et al.*[40]. The research work showed that free energy barrier for translocation of a melittin from the bilayer edge to the membrane surface was highly dependent on the number of inserted melittin peptides, and the barrier can be less than 4 kJ/mol when 5−7 melittins form a pore. This suggested that, once a membrane pore induced by multiple (5−7) peptides, the exchange of a single melittin peptide between pore and surface states is relatively easy. Our free energy results suggest, on the other hand, that the stability of pore is dependent on the number of peptides associated with the pore. Thus, by loosing a few melittin peptides around the bilayer edge, the pore can be destabilized. In this way, the melittin pore could be transient (especially in the experimental time frame).

5. Conclusions

We have performed a series of MD simulations to estimate the free energy barrier required to form a membrane pore in the presence/absence of multiple

melittin peptides. In the case of a pure lipid membrane, the free energy minimum only appeared at $\xi = 0$, which demonstrates that the unperturbed membrane (without pores) is the only stable state. On the other hand, in the free energy profiles reconstructed in the presence of 4, 5, 6, and 7 melittin peptides, the free energy minima at stable pore states were observed. The free energy barrier for pore formation is only a few $k_{\mathrm{B}}T$ in the presence of 6 or 7 melittin peptides. In these cases, the pore state was found at the free energy minimum. The stable pore radii were changed depending on the number of melittin peptides. The radius of 2.2 nm computed when six melittin peptides are present was in good agreement with the experimental pore radius obtained in a dehydrated DSPC membrane [48]. The line tension of the ribbon membrane was not equal to zero even if the local concentration of melittin peptides at the bilayer rim is higher than that of the stable pore. This is because melittin peptides have preferred the curvature of the bilayer rim to stabilize the pore. The free energy analysis for the insertion of a melittin peptide into the bilayer shows that a large free energy barrier must be overcome by a melittin peptide to bridge across the lipid membrane by the melittin peptide. This result suggests that a pore formation process most likely takes place in the presence of 6 or 7 melittin peptides in comparison to one-by-one melittin insertion. It should be noted that the present analyses have been performed starting from an initial configuration in which melittin peptides were ideally aligned on the membrane surface to encourage the pore formation. However, the series of analyses conducted here are quite useful to quantitatively evaluate the process of toroidal pore formation process driven by antimicrobial peptides, and will be helpful in determining the effect caused by different types of lipids and antimicrobial peptides on this process.

Acknowledgements

This research was partly supported by MEXT as "Priority Issue on Post-K computer" (Building Innovative Drug Discovery Infrastructure Through Functional Control of Biomolecular Systems). The calculations were performed using the facilities of Research Center for Computational Science, Okazaki and the Institute for Solid State Physics, the University of Tokyo.

References

[1] T. Y. Tsong, Electroporation of cell membranes, Biophys. J. 60 (1991) 297–306.

[2] V. Levadny, T. Tsuboi, M. Belaya, M. Yamazaki, Rate constant of tension-induced pore formation in lipid membranes, Langmuir 29 (2013) 3848–3852.

[3] K. Matsuzaki, Why and how are peptide-lipid interactions utilized for self-defense? Magainins and tachyplesins as archetypes, Biochim. Biophys. Acta 1462 (1999) 1–10.

[4] K. A. Brogden, Antimicrobial peptides: Pore formers or metabolic inhibitors in bacteria?, Nature Rev. Microbiol. 3 (2005) 238–250.

[5] L. T. Nguyen, E. F. Haney, H. J. Vogel, The expanding scope of antimicrobial peptide structures and their modes of action, Trends Biotechnol. 29 (2011) 464–472.

[6] M. Tosteson, D. Tosteson, The sting. melittin forms channels in lipid bilayers, Biophys. J. 36 (1981) 109–116.

[7] H. Vogel, F. Jähnig, The structure of melittin in membranes, Biophys. J. 50 (1986) 573–582.

[8] C. E. Dempsey, The actions of melittin on membranes, Biochim. Biophys. Acta 1031 (1990) 143–161.

[9] T. Katsu, C. Ninomiya, M. Kuroko, H. Kobayashi, T. Hirota, Y. Fujita, Action mechanism of amphipathic peptides gramicidin S and melittin on erythrocyte membrane, Biochim. Biophys. Acta 939 (1988) 57–63.

[10] K. Matsuzaki, S. Yoneyama, K. Miyajima, Pore formation and translocation of melittin, Biophys. J. 73 (1997) 831–838.

[11] B. Bechinger, Structure and functions of channel-forming peptides: Magainins, cecropins, melittin and alamethicin, J. Membr. Biol. 156 (1997) 197–211.

[12] A. S. Ladokhin, M. E. Selsted, S. H. White, Sizing membrane pores in lipid vesicles by leakage of co-encapsulated markers: Pore formation by melittin, Biophys. J. 72 (1997) 1762–1766.

[13] A. S. Ladokhin, S. H. White, Folding of amphipathic alpha-helices on membranes: Energetics of helix formation by melittin, J. Mol. Biol. 285 (1999) 1363–1369.

[14] L. Yang, T. A. Harroun, T. M. Weiss, L. Ding, H. W. Huang, Barrel-stave model or toroidal model? A case study on melittin pores, Biophys. J. 81 (2001) 1475–1485.

[15] K. Hristova, C. E. Dempsey, S. H. White, Structure, location, and lipid perturbations of melittin at the membrane interface, Biophysical Journal 80 (2001) 801–811.

[16] M. T. Lee, F. Y. Chen, H. W. Huang, Energetics of pore formation induced by membrane active peptides, Biochemistry 43 (2004) 3590–3599.

[17] D. Allende, S. A. Simon, T. J. Mcintosh, Melittin-induced bilayer leakage depends on lipid material properties: Evidence for toroidal pores, Biophys. J. 88 (2005) 1828–1837.

[18] A. J. Krauson, J. He, W. C. Wimley, Gain-of-function analogues of the pore-forming peptide melittin selected by orthogonal high-throughput screening, J. Am. Chem. Soc. 134 (2012) 12732–12741.

[19] X. Chen, J. Wang, A. P. Boughton, C. B. Kristalyn, Z. Chen, Multiple orientation of melittin inside a single lipid bilayer determined by combined vibrational spectroscopic studies, J. Am. Chem. Soc. 129 (2007) 1420–1427.

[20] H. Raghuraman, A. Chattopadhyay, Melittin: A membrane-active peptide with diverse functions, Bioscience Rep. 27 (2007) 189–223.

[21] G. V. D. Bogaart, J. V. Guzmán, J. T. Mika, B. Poolman, On the mechanism of pore formation by melittin, J. Biol. Chem. 283 (2008) 33854–33857.

[22] G. Klocek, T. Schulthess, Y. Shai, J. Seelig, Thermodynamics of melittin binding to lipid bilayers. Aggregation and pore, Biochemistry 48 (2009) 2586–2596.

[23] A. S. Ladokhin, M. Fernández-Vidal, S. H. White, CD spectroscopy of peptides and proteins bound to large unilamellar vesicles, J. Membr. Biol. 236 (2010) 247–253.

[24] A. J. Krauson, J. He, W. C. Wimley, Determining the mechanism of membrane permeabilizing peptides: Identification of potent, equilibrium pore-formers, Biochim. Biophys. Acta 1818 (2012) 1625–1632.

[25] J.-H. Lin, A. Baumgaertner, Stability of a melittin pore in a lipid bilayer: A molecular dynamics study, Biophys. J. 78 (2000) 1714–1724.

[26] D. Sengupta, H. Leontiadou, A. E. Mark, S. J. Marrink, Toroidal pores formed by antimicrobial peptides show significant disorder, Biochim. Biophys. Acta 1778 (2008) 2308–2317.

[27] M. Manna, C. Mukhopadhyay, Cause and effect of melittin-induced pore formation: A computational approach, Langmuir 25 (2009) 12235–12242.

[28] M. Mihajlovic, T. Lazaridis, Antimicrobial peptides in toroidal and cylindrical pores, Biochim. Biophys. Acta 1798 (2010) 1485–1493.

[29] K. P. Santo, M. L. Berkowitz, Difference between bagainin-2 and melittin assemblies in phosphatidylcholine bilayers: Results from coarse-grained simulations, J. Phys. Chem. B 116 (2012) 3021–3030.

[30] S. J. Irudayam, M. L. Berkowitz, Binding and reorientation of melittin in a POPC bilayer: Computer simulations, Biochim. Biophys. Acta 1818 (2012) 2975–2981.

[31] M. Mihajlovic, T. Lazaridis, Charge distribution and imperfect amphipathicity affect pore formation by antimicrobial peptides, Biochim. Biophys. Acta 1818 (2012) 1274–1283.

[32] K. P. Santo, S. J. Irudayam, M. L. Berkowitz, Melittin creates transient pores in a lipid bilayer: Results from computer simulations, J. Phys. Chem. B 117 (2013) 5031–5042.

[33] S. J. Irudayam, T. Pobandt, M. L. Berkowitz, Free energy barrier for melittin reorientation from a membrane-bound state to a transmembrane state, J. Phys. Chem. B 117 (2013) 13457–13463.

[34] Y. Hu, S. K. Sinha, S. Patel, Investigating hydrophilic pores in model lipid bilayers using molecular simulations: Correlating bilayer properties with pore-formation thermodynamics, Langmuir 31 (2015) 6615–6631.

[35] J. M. Leveritt III, A. Pino-Angeles, T. Lazaridis, The structure of a melittin-stabilized pore, Biophys. J. 108 (2015) 2424–2426.

[36] D. Sun, J. Forsman, C. E. Woodward, Amphipathic membrane-active peptides recognize and stabilize ruptured membrane pores: Exploring cause and effect with coarse-grained simulations, Langmuir 31 (2015) 752–761.

[37] D. Sun, J. Forsman, C. E. Woodward, Multistep molecular dynamics simulations identify the highly cooperative activity of melittin in recognizing and stabilizing membrane pores, Langmuir 31 (2015) 9388–9401.

[38] Y. Lyu, X. Zhu, N. Xiang, G. Narsimhan, Molecular dynamics study of pore formation by melittin in a 1,2-dioleoyl-*sn*-glycero-3-phosphocholine and 1,2-di(9Z-octadecenoyl)-sn-glycero-3-phospho-(1'-*rac*-glycerol) mixed lipid bilayer, Ind. Eng. Chem. Res. 54 (2015) 10275–10283.

[39] D. Sun, J. Forsman, E. Woodward, Molecular simulations of melittin-induced membrane pores, J. Phys. Chem. B 121 (2017) 10209–10214.

[40] Y. Lyu, N. Xiang, X. Zhu, G. Narsimhan, Potential of mean force for insertion of antimicrobial peptide melittin into a pore in mixed DOPC/DOPG lipid bilayer by molecular dynamics simulation, J. Chem. Phys. 146 (2017) 155101.

[41] J. B. Klauda, R. M. Venable, J. A. Freites, J. W. O'Connor, D. J. Tobias, C. Mondragon-Ramirez, I. Vorobyov, A. D. MacKerell, R. W. Pastor, Update of the CHARMM all-atom additive force field for lipids: Validation on six lipid types, J. Phys. Chem. B 114 (2010) 7830–7843.

[42] R. B. Best, X. Zhu, J. Shim, P. E. Lopes, J. Mittal, M. Feig, A. D. MacKerell, Optimization of the additive CHARMM all-atom protein force field targeting improved sampling of the backbone ϕ, ψ and side-chain $\chi1$ and $\chi2$ dihedral angles, J. Chem. Theory Comput. 8 (2012) 3257–3273.

[43] A. Botan, F. Favela-Rosales, P. F. Fuchs, M. Javanainen, M. Kanduč, W. Kulig, A. Lamberg, C. Loison, A. Lyubartsev, M. S. Miettinen, L. Monticelli, J. Määttä, O. H. Ollila, M. Retegan, T. Róg, H. Santuz,

J. Tynkkynen, Toward atomistic resolution structure of phosphatidylcholine headgroup and glycerol backbone at different ambient conditions, J. Phys. Chem. B 119 (2015) 15075–15088.

[44] Y. Wang, T. Zhao, D. Wei, E. Strandberg, A. S. Ulrich, J. P. Ulmschneider, How reliable are molecular dynamics simulations of membrane active antimicrobial peptides?, Biochim. Biophys. Acta 1838 (2014) 2280–2288.

[45] W. F. D. Bennett, C. K. Hong, Y. Wang, D. P. Tieleman, Antimicrobial peptide simulations and the influence of force field on the free energy for pore formation in lipid bilayers, J. Chem. Theory Comput. 12 (2016) 4524–4533.

[46] M. Andersson, J. P. Ulmschneider, M. B. Ulmschneider, S. H. White, Conformational states of melittin at a bilayer interface, Biophys. J. 104 (2013) L12–L14.

[47] C. H. Chen, G. Wiedman, A. Khan, M. B. Ulmschneider, Absorption and folding of melittin onto lipid bilayer membranes via unbiased atomic detail microsecond molecular dynamics simulation, Biochim. Biophys. Acta 1838 (2014) 2243–2249.

[48] M. T. Lee, T. L. Sun, W. C. Hung, H. W. Huang, Process of inducing pores in membranes by melittin, Proc. Natl. Acad. Sci. U.S.A. 110 (2013) 14243–14248.

[49] R. A. Böckmann, A. Hac, T. Heimburg, H. Grubmüller, Effect of Sodium Chloride on a Lipid Bilayer, Biophys. J. 85 (2003) 1647–1655.

[50] H. Raghuraman, A. Chattopadhyay, Effect of Ionic Strength on Folding and Aggregation of the Hemolytic Peptide Melittin in Solution, Biopolymers 83 (2006) 111–121.

[51] S. Jo, T. Kim, V. G. Iyer, W. Im, CHARMM-GUI: A web-based graphical user interface for CHARMM, J. Comput. Chem. 29 (2008) 1859–1865.

[52] T. C. Terwilliger, D. Eisenberg, The structure of melittin. I. Structure determination and partial refinement, J. Biol. Chem. 257 (1982) 6010–6015.

[53] I. Kabelka, R. Vácha, Optimal conditions for opening of membrane pore by amphiphilic peptides, J. Chem. Phys. 143 (2015) 243115.

[54] M. J. Abraham, T. Murtola, R. Schulz, S. Páll, J. C. Smith, GROMACS: High performance molecular simulations through multi-level parallelism from laptops to supercomputers, SoftwareX 1-2 (2015) 19–25.

[55] W. L. Jorgensen, J. Chandrasekhar, J. D. Madura, R. W. Impey, M. L. Klein, Comparison of simple potential functions for simulating liquid water, J. Chem. Phys. 79 (1983) 926–935.

[56] S. Nosé, A unified formulation of the constant temperature molecular dynamics methods, J. Chem. Phys. 81 (1984) 511–519.

[57] W. G. Hoover, Canonical dynamics: Equilibrium phase-space distributions, Phys. Rev. A 31 (1985) 1695–1697.

[58] M. Parrinello, A. Rahman, Polymorphic transitions in single crystals : A new molecular dynamics method, J. Appl. Phys. 52 (1981) 7182–7190.

[59] T. Darden, D. York, L. Pedersen, Particle mesh Ewald - An N.log(N) method for Ewald sums in large systems, J. Chem. Phys. 98 (1993) 10089–10092.

[60] U. Essmann, L. Perera, M. L. Berkowitz, T. Darden, H. Lee, L. G. Pedersen, A smooth particle mesh Ewald method, J. Chem. Phys. 103 (1995) 8577–8593.

[61] B. Hess, H. Bekker, H. J. C. Berendsen, LINCS: a linear constraint solver for molecular simulations, J. Comput. Chem. 18 (1997) 1463–1472.

[62] T. V. Tolpekina, W. K. den Otter, W. J. Briels, Nucleation free energy of pore formation in an amphiphilic bilayer studied by molecular dynamics simulations, J. Chem. Phys. 121 (2004) 12060–12066.

[63] G. M. Torrie, J. P. Valleau, Nonphysical sampling distributions in Monte Carlo free-energy estimation: Umbrella sampling, J. Comput. Phys. 23 (1977) 187–199.

[64] S. Kumar, J. M. Rosenberg, D. Bouzida, R. H. Swendsen, P. A. Kollman, The weighted histogram analysis method for free-energy calculations on biomolecules. I. The method, J. Comput. Chem. 13 (1992) 1011–1021.

[65] J. S. Hub, N. Awasthi, Probing a continuous polar defect: A reaction coordinate for pore formation in lipid membranes, J. Chem. Theory Comput. 13 (2017) 2352–2366.

[66] F. Y. Jiang, Y. Bouret, J. T. Kindt, Molecular dynamics simulations of the lipid bilayer edge., Biophys. J. 87 (2004) 182–192.

[67] A. Pino-angeles, T. Lazaridis, Effects of Peptide Charge , Orientation , and Concentration on Melittin Transmembrane Pores, Biophys. J. 114 (2018) 2865–2874.

[68] T. Portet, R. Dimova, A new method for measuring edge tensions and stability of lipid bilayers: Effect of membrane composition, Biophys. J. 99 (2010) 3264–3273.

[69] W. Shinoda, T. Nakamura, S. O. Nielsen, Free energy analysis of vesicle-to-bicelle transformation, Soft Matter 7 (2011) 9012–9020.

[70] R. Devane, W. Shinoda, P. B. Moore, M. L. Klein, Transferable coarse grain nonbonded interaction model for amino acids, J. Chem. Theory Comput. 5 (2009) 2115–2124.

[71] W. Shinoda, R. Devane, M. L. Klein, Zwitterionic lipid assemblies: Molecular dynamics studies of monolayers, bilayers, and vesicles using a new coarse grain force field, J. Phys. Chem. B 114 (2010) 6836–6849.

[72] S. Seo, W. Shinoda, Spica force field for lipid membranes: Doamin formation induced by cholesterol, J. Chem. Theory Comput. (2018) DOI: 10.1021/acs.jctc.8b00987.